Pharm Res (2011) 28:1884–1894
DOI 10.1007/s11095-011-0416-7

RESEARCH PAPER

Aggregation Stability of a Monoclonal Antibody During Downstream Processing

Paolo Arosio • Giuliano Barolo • Thomas Müller-Späth • Hua Wu • Massimo Morbidelli

Received: 22 December 2010 / Accepted: 3 March 2011 / Published online: 30 March 2011

ABSTRACT

Purpose To study the effect of several operative parameters, particularly pH and salt concentration, on the stability and aggregation kinetics of IgG solutions under the conditions typically encountered in downstream processing.

Methods The time evolution of the aggregates is analyzed by a combination of dynamic light scattering, size exclusion chromatography (SEC) and field flow fractionation (FFF). Secondary structure changes are monitored by circular dichroism.

Results For the given antibody, it is found that at pH lower than 4.0 addition of salt induces a reversible aggregation to oligomers accompanied by an increase in the content of the β-sheet structure. The aggregation rate increases monotonically with the salt concentration. Both the SEC and FFF techniques are successfully applied to obtain the oligomer distributions, and their results are consistent. The modified Lumry-Eyring kinetic model can well describe the time evolutions of the oligomers.

Conclusions For the given antibody, low pH and presence of salt induce conformational changes that are responsible for the reversible aggregation, but in the investigated conditions only small soluble oligomers are formed and oligomer sizes larger than trimer are negligible. For this reason, no accompanied macroscopic changes can be observed.

KEY WORDS aggregation · antibody · FFF· oligomer distribution · SEC

Electronic supplementary material The online version of this article (doi:10.1007/s11095-011-0416-7) contains supplementary material, which is available to authorized users.

P. Arosio · G. Barolo · T. Müller-Späth · H. Wu · M. Morbidelli (✉)
Department of Chemistry and Applied Biosciences
Institute for Chemical and Bioengineering, ETH Zurich
8093 Zurich, Switzerland
e-mail: massimo.morbidelli@chem.ethz.ch

INTRODUCTION

Thanks to increased understanding of the biological background of various human diseases, protein drugs have been increasingly developed and now occupy a significant part of the whole pharmaceutical market (1). Particularly, monoclonal antibodies represent the most rapidly growing product inside the family of recombinant therapeutic proteins (2). The successful commercialization of protein drug is often limited by instability problems, which can be both chemical (e.g., deamidation, oxidation, hydrolysis) and physical (e.g., conformational changes, adsorption to surfaces, aggregation) (3,4). Protein aggregation represents the most common form of all possible deteriorations and can basically be encountered in each step of the production process (5). The spectrum of the possible products resulting from aggregation is wide. The several types of aggregates may be classified in covalent/non-covalent, reversible/irreversible, native/denatured, soluble/non-soluble (6,7).

Obviously, protein aggregation in pharmaceutical products must be avoided, since it usually leads to inactivation of the drug and can even trigger an immunogenic reaction of the organism. Since the debate on the possible immunoresponse created by aggregates is still open (8,9), strict specification limits are imposed by the drug manufacturers as a precaution. Shelf-life prediction is a challenging problem for pharmaceutical companies, since several external factors may induce protein instability (4,7) during production, storage, transportation and handling of the pharmaceutical component: temperature (10), buffer formulation (pH, presence of solutes, co-solvents, surfactants, salts) (11), mechanical stress (12,13) and surface interaction (14). Such environmental factors affect at a molecular level the protein-protein and protein-salt interactions (15) with consequences on the two main aspects involved in the

aggregation process: the colloidal stability of the protein solution and the thermodynamic folding of the protein (4). The two processes are strictly connected one to another and are often inseparable.

Protein aggregation is associated to more than 20 human disorders (16), most of which are neurodegenerative diseases like Prion diseases (17), Alzheimer's disease, Parkinson's disease, sickle cell disease and Huntington's disease. Typically, in such biological systems proteins aggregate into large insoluble fibrils through nucleation-dependent assembly, even if in some cases also amorphous deposits are observed. Although great attention has been given in the literature to understand these diseases, the mechanism leading to the formation of such fibrils is unclear, and validated treatments are still missing. Achieving a better understanding of the mechanisms responsible for protein aggregation is crucial for the development of an effective pharmaceutical treatment of the aforementioned diseases. While the mechanism leading to amyloid fibrils is the object of large investigation in the literature, relatively few papers have tried to elucidate the aggregation pathway of monoclonal antibodies (18–20).

In this work, we focus on the aggregation of an IgG immunoglobulin during its production process and specifically on the downstream, i.e. the purification portion of it. In particular, we investigate the conditions relevant for Protein A chromatography, which represents the typical capture process in antibodies purification (21). The effect of several operating parameters (i.e., pH, protein concentration, buffer nature, concentration of salts) on the protein solution stability is investigated. The main focus of this work is on antibody oligomer formation and distribution. Since each technique has its own limits and advantages and often cannot be used alone to detect the aggregation process (7,22), the oligomer formation and distribution have been continuously followed on-line by dynamic light scattering (DLS) and off-line by size exclusion chromatography (SEC) and asymmetric field flow fractionation (FFF). Circular dichroism (CD) studies were also performed to correlate aggregation tendency with change in protein secondary structure. Moreover, the comparison between on-line and off-line data can give important information about the reversibility of the aggregation. The obtained oligomer information during aggregation is then modelled in the frame of a modified Lumry-Eyring model (23–25), which considers the native monomers to reversibly unfold into a partially unfolded, aggregation-prone state (26).

The present work represents also a general procedure for analyzing protein oligomers, which, produced in the early stages of the aggregation, are considered to be crucial, toxic species in many diseases (27). An example is represented by the amyloidosis diseases related to aggregation of light chains of antibodies (28). Since the size of the light chain fragments is not much different from that of the complete antibody and the two proteins share common characteristics, the approach described in this work may be used to detect light chain oligomers during aggregation.

MATERIALS AND METHODS

Antibodies and Chemicals

The monoclonal IgG antibody employed in this work is an IgG 2, with MW ~150 kDa and the isoelectric point (pI) between 7.35 and 8.15, supplied by Merck Serono (Vevey, Switzerland).

The buffers used for all experiments were a 25 mM citric acid solution and a 25 mM acetic acid solution, both at pH 3.0. In order to prevent formation and proliferation of bacteria during storage, 1.0 g/L of sodium azide was added to the buffers. All buffers were filtered with 0.45 μm cut-off, Durapore membrane filters (Millipore, Billerica, MA, USA).

Dynamic Light Scattering

The average size of the aggregates or oligomers was measured on-line by the *in-situ* dynamic light scattering (DLS) technique, using a Zetasizer Nano (Malvern, UK). The original antibody concentration was 12 g/L, which was then diluted to 1 g/L by a selected buffer solution with proper pH and ionic strength to monitor formation of the oligomers. All samples were filtered with a 0.02 μm cut-off, Anotop 10 syringe filter (Whatman, Kent, UK), before starting the aggregation. Micro UV-Cuvettes with dimension 12.5×12.5×45 mm (70 μL) and light path 1 cm (Brand GmbH, Wertheim, Germany) were used for the DLS measurements. For each investigated condition, three independent samples were prepared and analyzed. For a single sample, the size at a given time is the repetition of three measurements. The reported values are the average of the three independent experiments.

Size Exclusion Chromatography

During the DLS experiments, samples were taken and analyzed by the size exclusion chromatography (SEC) technique with a Superdex 200 10/300 GL, 10 mm× 300 mm size-exclusion column (GE Healthcare, Uppsala, Sweden) assembled on a Agilent 1200 series HPLC unit (Santa Clara, CA, USA) consisting of a quaternary pump with degasser, an autosampler with a cooling unit, a column oven, and a DAD detector. Each sample was eluted for 60 min at a constant flow rate of 0.5 mL/min using as mobile phase a 100 mM sodium sulphate, 25 mM Na_2HPO_4 solution at pH 7.0, filtered with a 0.45 μm cut-

off, Durapore membrane filter (Millipore, Billerica, MA, USA). The UV absorbance peaks were detected at 280 nm and 220 nm.

Field Flow Fractionations

Paralleling with the SEC technique, the field flow fractionations (FFF) technique was also used to analyze the oligomer composition. The applied instrument was an AF4 Eclipse 3+ (Wyatt, Santa Barbara, CA, USA), coupled with a 1200 Series isocratic pump from Agilent (Santa Clara, CA, USA). A 275 mm LC channel for aqueous solvents was used for Eclipse 3, with a trapezoidal spacer (350 μm thick, 26.5 cm long) and a Nadir reg. cellulose membrane with 10 kDa cut-off at the bottom (Wyatt, Dernbach, Germany). The detector flow was set constant at 1 mL/min, and a step gradient of cross flow from 5 ml/min to 0 ml/min was applied after 30 min (29). Twenty five mM citric acid solution at pH 3.0 was used as mobile phase, after filtration through a 0.1 μm cur-off, Durapore membrane filter (Millipore, Billerica, MA, USA).

Circular Dichroism (CD)

For the variations in the secondary structure of the antibody during aggregation, we have monitored the Far-UV circular dichroism (CD) spectra of the same antibody solutions using a Jasco-815 CD spectrophotometer (Mary's Court, Easton, MD) with the temperature of the cell holder controlled at 25°C. A quartz cuvette with 0.1 cm path length was used.

RESULTS

pH Effect

As already mentioned in the Introduction, protein A affinity chromatography is commonly used as the capture step for purification of monoclonal antibodies and Fc fusion proteins in drug industry. The recovery of the product bound to the stationary phase requires the elution with a low pH mobile phase (usually between pH 3.0 and 4.0) (21), which is well known to potentially induce aggregation (19). Particularly, low pH values can lead to changes in the structure of the Fc domain, while Fab fragments have been shown to be more sensitive to temperature variations (30). Moreover, highly concentrated antibody solutions, which are desired for the economy of large-scale purification processes, further increase the risk of inducing aggregation under low pH conditions. The effect of pH was first investigated for a solution of 1 g/L mAb in 25 mM citric acid buffer with 0.15 M NaCl (a buffer commonly used in protein A chromatography) at several pH values. The stability of such solutions was followed on-line by *in-situ* DLS. The time evolution of the average hydrodynamic radius $\langle R_h \rangle$ of the distribution of mAb monomers and oligomers is shown in Fig. 1a. For pH values between 4.5 and 6.0, the solutions are very stable ($\langle R_h \rangle = 6$ nm is in fact the value corresponding to the monomer mAb under examination), while aggregation occurs when pH drops below a critical value of about 4.0. It is worth noting that the extent of the aggregation in all cases is independent of pH.

Moreover, for all cases where aggregation occurs, the aggregation starts immediately after incubation without any

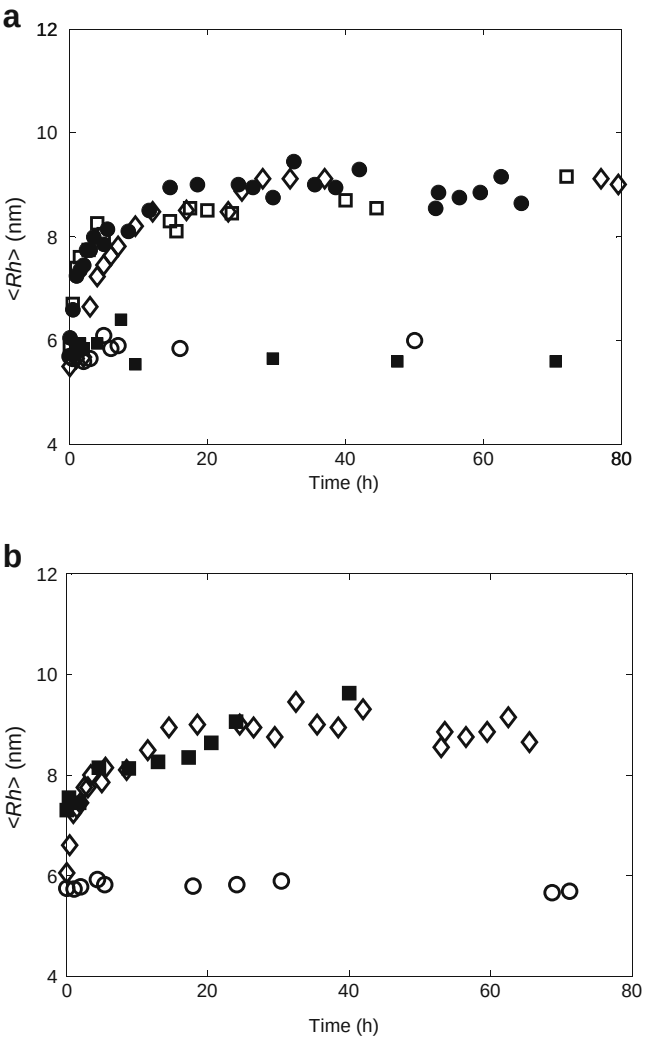

Fig. 1 (**a**) Time evolutions of the average hydrodynamic radius $\langle R_h \rangle$, measured on-line by *in-situ* DLS, for the 1 g/L mAb solution in 25 mM citric acid buffer with 0.15 M NaCl, at pH 3.0 (●), 3.5 (□), 4.0 (◇), 4.5 (■) and pH 6 (○); (**b**) the same as (**a**) but for the 1 g/L mAb solution in 25 mM phospate buffer (○), 25 mM citric acid buffer (◇) and 25 mM acetic acid buffer (□) with 0.15 M NaCl at pH 3.0.

lag-time, which is commonly encountered in other protein aggregating systems. From the average $\langle R_h \rangle$ values shown in Fig. 1a, only small oligomers are produced (probably no more than 2 or 3 monomer units) and basically stop growing after about 1.5 h. No macroscopic changes in the solutions can in fact be observed even after 1 month of incubation.

Buffer and Salt Concentration Effect

To observe the effect of the ionic strength and the nature of the buffer on the mAb aggregation, several experiments at different salt concentrations and in different buffers (phosphate, citric acid and acetic acid buffer), but at a constant pH 3.0, were performed. The conditions for all the experimental runs are described in Table I.

The stability of the mAb solutions in the concentration range from 1 to 5 g/L was first checked in various buffers, typically used in protein A chromatography, without adding additional salts (runs 1 to 4 in Table I). All antibody solutions were stable after 4 weeks, with an average hydrodynamic radius of around 6 nm, which depends slightly on the type of buffer.

The addition of sodium chloride to different buffers leads to different consequences. Figure 1b shows the time evolution of $\langle R_h \rangle$ for 1 g/L mAb solutions at 0.15 M sodium chloride in three different buffers. In the case of phosphate buffer, the antibody solution remains stable for more than 3 weeks, while in acetate and citric acid buffers aggregation occurs with very similar kinetics and extent. Next, for the acetic and citric acid buffers, the effect of the NaCl concentration on mAb aggregation has been investigated in a large range of NaCl concentrations between 0 and 0.5 M. Figure 2 shows the time evolutions of $\langle R_h \rangle$ for the mAb solutions in the citric acid buffer at different salt concentrations (runs 4, 5, 6, 9 and 10 in Table I), and the corresponding CD spectra after 24 h of incubation are shown in Fig. 3a. It can be seen that as the salt concentration increases, the aggregation extent increases, and the minimum (at 217 nm) in the CD spectra, corresponding to the β-sheet structure of the immunoglobulin (30), moves downwards more and more, indicating that the aggregation is accompanied by an increase in the more ordered β-sheet structure content.

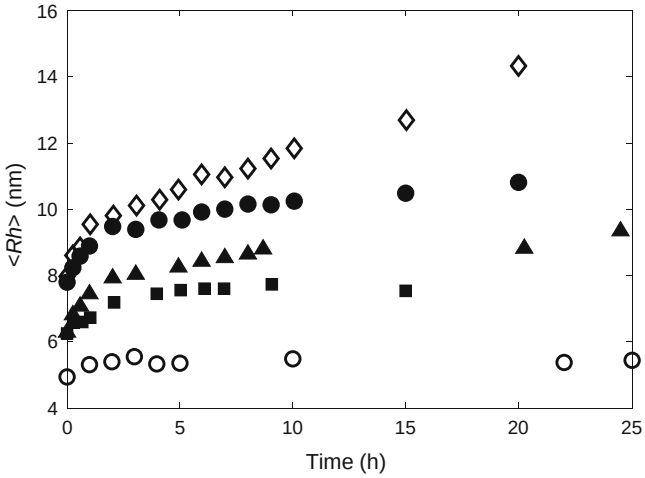

Fig. 2 Time evolutions of the average hydrodynamic radius, measured on-line by the *in-situ* DLS, for the 1 g/L mAb solution in 25 mM citric acid buffer at pH 3.0 and different salt contrentations: 0 M (○), 0.1 M (■), 0.15 M (▲), 0.3 M (●), 0.5 M (◇) (Runs 4, 5, 6, 9 and 10 in Table I).

In the case of 0.3 M NaCl in Fig. 2 (run 6 in Table I), the corresponding time evolution of the CD spectra has also been measured and shown in Fig. 3b. It is evident that the minimum in the CD spectra moves progressively downwards with time. However, after a few hours, the change in the spectra for different times (e.g., at 22 h and 48 h) becomes insignificant. This is consistent with the aggrega-

Table I Summary of Experimental Runs. All Experiments Were Performed at pH 3.0

Run	mAb Conc. (g/L)	Buffer	NaCl Conc. mol/L	Stability
1	1 to 5	25 mM Phosphate	0	Stable
2	1 to 5	0.1 M Glycine-HCl	0	Stable
3	1 to 5	25 mM-1 M Acetic Acid	0	Stable
4	1 to 5	25 mM Citric Acid	0	Stable
5	1	25 mM Citric Acid	0.1	Unstable
6	1	25 mM Citric Acid	0.15	Unstable
7	10	25 mM Citric Acid	0.15	Unstable
8	0.1	25 mM Citric Acid	0.15	Unstable
9	1	25 mM Citric Acid	0.3	Unstable
10	1	25 mM Citric Acid	0.5	Unstable
11	1	25 mM Acetic Acid	0.1	Unstable
12	1	25 mM Acetic Acid	0.15	Unstable
13	1	25 mM Acetic Acid	0.3	Unstable
14	1	25 mM Acetic Acid	0.5	Unstable

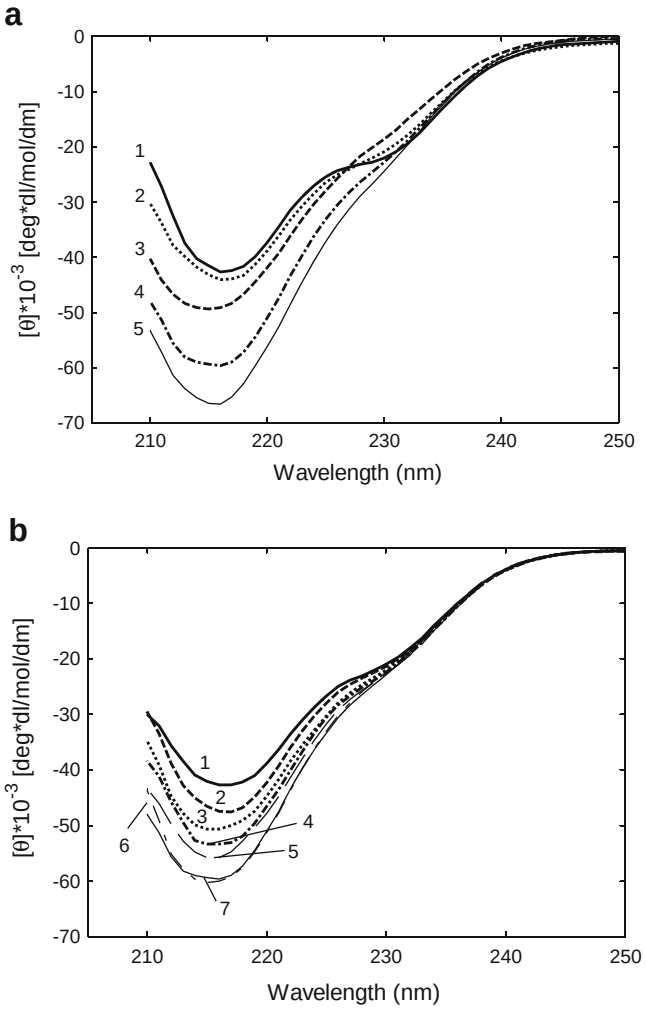

Fig. 3 (**a**) CD spectra for the 1 g/L mAb soltuion in 25 mM citric buffer at pH 3.0, after 1 day incubation at different salt contrentations: 0 M (1), 0.1 M (2), 0.15 M (3), 0.3 M (4), 0.5 M (5); (**b**) CD spectra for Case 3 in (**a**), measured at different aggregation times: 0 min (1), 10 min (2), 30 min (3), 50 min (4), 90 min (5), 22 h (6), 48 h (7).

tion extent measured by DLS in Fig. 2, indicating that antibody aggregation and change in secondary structure occur simultaneously.

In the case of the acetic acid buffer, the observed aggregation behavior and changes in the secondary structure for the experimental runs 11 to 14 in Table I are very similar to those shown above in the case of the citric acid buffer. Thus, for brevity, the data are not shown, but the conclusions reached above are also valid for the acetic acid buffer. On the other hand, this is not the case for the phosphate buffer where, as shown in Fig. 1b, no aggregation occurs.

Oligomer Distribution

Samples at different incubation times were taken and analyzed by SEC and FFF. Examples of the obtained oligomer distribution are shown in Fig. 4, corresponding to run 6 in Table I. The distributions obtained from the two techniques are consistent (note that in FFF larger species elute after smaller ones, while in SEC they elute in opposite order). At time = 0, only the monomers and a small (negligible) fraction of dimers are present. After 3 h incubation, a sharp decrease in the monomer concentration and formation of a significant quantity of dimers can be observed. However, after the first few hours, both the FFF and SEC chromatograms show that the concentrations of both monomers and dimers vary very slowly, which is in good agreement with the DLS data in Fig. 1 and the CD spectra in Fig. 3b.

In the FFF chromatograms in Fig. 4a the dimer peaks are asymmetrical and not well separated from the peaks of trimers and larger species, while the separation is much more clear in the SEC chromatograms. Nevertheless, a clear shoulder around the elution time of 15 min can be observed, representing proper separation between dimers

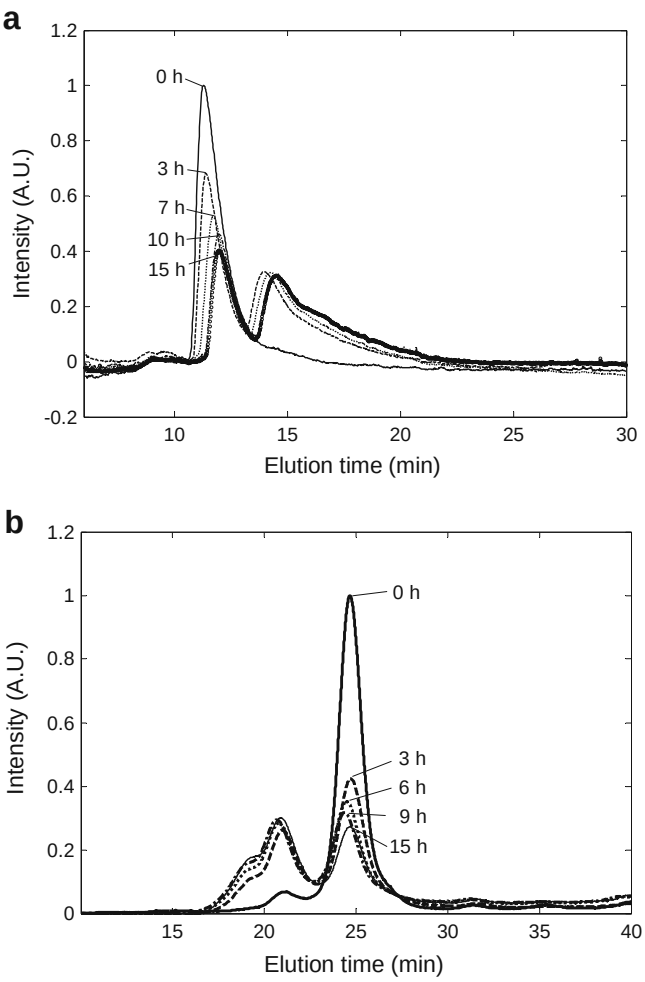

Fig. 4 (**a**) FFF chromatograms at different times along the aggregation for run 6 in Table I; (**b**) SEC chromatograms at different times for the same system in (**a**).

and trimers. From both the SEC and FFF chromatograms, the mass fractions of each species can be evaluated based on the ratio of the area under the corresponding peak and the total area. The underlying assumption of such approach is that the absorbance capacity of the oligomers depends linearly on their size, i.e., a dimer absorbs twice as a monomer, a trimer three times, and so forth. As a confirmation of this assumption, in all the experimental runs the total area remained constant along the aggregation time, in both SEC and FFF techniques.

It is known that both SEC and FFF can be affected by several parameters during the analysis, such as interactions between proteins and the stationary phase, dilution effect of the injected sample, shear-induced aggregation during the focus mode of FFF, etc. Thus, it is important to check the reliability of the obtained distributions. Moreover, comparing the results from different techniques can give information about the strength of the formed aggregates and their reversibility. For example, weakly aggregated oligomers would be destroyed easily upon dilution during the SEC or FFF analysis, and the obtained distributions would be inconsistent with the on-line DLS measurements. To verify this, we have coupled an on-line DLS system (Wyatt, Dernbach, DE) with the SEC column, so as to estimate the hydrodynamic radius, R_h, of dimer and trimer, which were found to be equal to 7.3 and 9.7 nm, respectively. These values were then used to calculate the time evolution of the Z-average hydrodynamic radius of the same system based on the following well-known relationship (31):

$$\langle R_h \rangle = \frac{\sum_1^N n_i(t) \cdot i^2}{\sum_1^N \frac{n_i(t) \cdot i^2}{R_{h,i}}} \tag{1}$$

where i is mass of the oligomer (i.e., the number of the monomeric mAbs forming the oligomer), while n_i and $R_{h,i}$ are the number concentration and the hydrodynamic radius of the oligomer with mass i, respectively. In particular, in the $\langle R_h \rangle$ computations using Eq. 1 for each corresponding system, we have applied the oligomer distributions n_i that are determined from the analyses of the SEC and FFF techniques, respectively. In Fig. 5, we have compared such computed time evolutions of $\langle R_h \rangle$ to those measured directly on-line by the *in-situ* DLS technique, in the cases of run 6 and run 9 in Table I. It can be seen that the agreement between the three techniques is very good. Therefore, the obtained oligomer distributions from the SEC and FFF techniques are reliable and reflect the true oligomer distributions in the system. Moreover, these results indicate that the oligomers formed during aggregation are strong enough to survive during the SEC and FFF fractionation processes.

Furthermore, we have also investigated the long-term reversibility of the aggregation process. To this aim, we have collected two samples after 4 h incubation in the case of run 7 in Table I: one sample was immediately analyzed by SEC, while another was diluted ten-fold in a salt-free citric acid buffer, so as to alter the equilibrium, and analyzed by SEC after 1 h and after 48 h. The results, shown in Fig. 6, indicate that aggregation is indeed reversible, and the monomers can be recovered by dilution in a salt-free buffer. It should be pointed out, however, that further investigations are required to understand whether the recovered monomers have the original secondary structure or keep the same structure as in the oligomers.

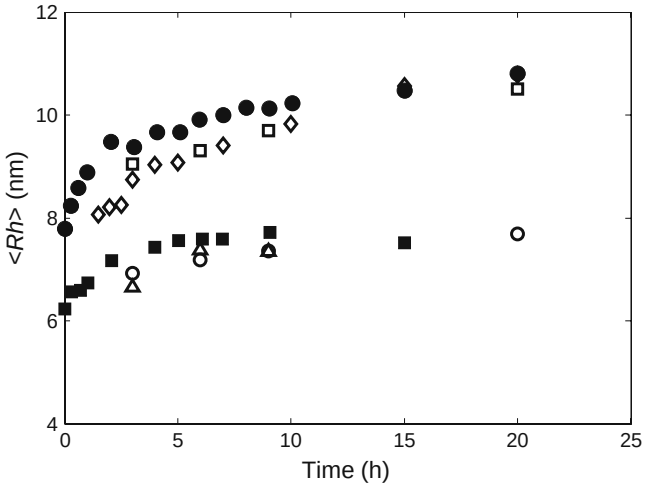

Fig. 5 Time evolutions of the average hydrodynamic radius measured on-line by the *in-situ* DLS for runs 6 and 9 in Table I, compared with those reconstructed from the oligomer distribution data obtained from FFF and SEC techniques. Run 6: DLS (■), SEC (○), FFF (△); Run 9: DLS (●), SEC (□), FFF (◇).

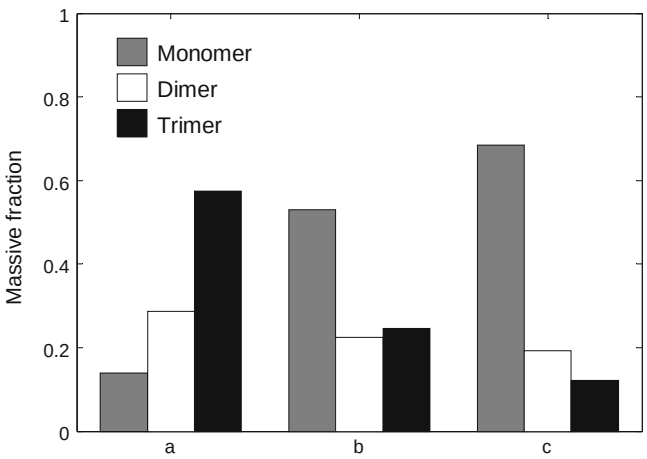

Fig. 6 Distributions of the oligomers determined from the SEC technique for (**a**) sample from run 7 in Table I after 4 h incubation, (**b**) the same as (**a**) but diluted to 1 g/L mAb concentration in 25 mM citric acid buffer at pH 3.0 without adding salt and the analysis performed after 1 h, and (**c**) the same as (**b**) but the analysis performed after 48 h.

DISCUSSION

Kinetic Modelling of the Oligomer Formation

Protein aggregation induced by conformational changes is commonly described by the Lumry-Eyring model, developed in 1954 (23). According to this model, a native protein unfolds in a reversible way into an unfolded state which then aggregates irreversibly. Several recent studies published in the literature showed that not only the completely unfolded species but also different types of intermediates (near native (32,33) or partly folded (34,35)) can be the aggregation-prone form of the monomeric species.

In the present work, following the approach of Roberts (24), we modify the Lumry-Eyring model to describe the mAb aggregation process, by taking into account the reversibility of each step. The main assumptions involved in the model are the following:

- A unique reactive intermediate prone to aggregation is present, indicated as *I*. With respect to the aggregation process, the intermediate (I) and native (N) species can reach thermodynamic equilibrium instantaneously, which can be described through the equilibrium constant $K_{eq} = k_{unf}/k_{fold}$.
- Two I species can aggregate to form a dimer (D). Larger oligomers are formed only by subsequent addiction of an I unit, while aggregation between two oligomers has been neglected.
- Since the observed oligomers larger than trimer are negligible, trimers (T) have been considered as the largest species present in the system.
- All the aggregation steps have been considered reversible and characterized by intrinsic forward and backward rate constants. Note that reversibility was not taken into account in the original Lumry-Eyring model, but it has been observed in several studies (25,36).

The resulting reaction scheme is shown in Fig. 7, based on which the following mass balances can be derived:

$$\frac{d[N]}{dt} = -k_{unf}[N] + k_{fold}[I] \tag{2}$$

$$\frac{d[I]}{dt} = k_{unf}[N] - k_{fold}[I] - 2k_1[I]^2 + 2k_{-1}[D] - k_2[I][D] + k_{-2}[T] \tag{3}$$

$$\frac{d[D]}{dt} = k_1[I]^2 - k_{-1}[D] - k_2[I][D] + k_{-2}[T] \tag{4}$$

$$\frac{d[T]}{dt} = k_2[I][D] - k_{-2}[T] \tag{5}$$

$$N \underset{}{\overset{K_{eq}}{\rightleftarrows}} I$$

$$K_{eq} = \left(\frac{[I]}{[N]}\right)_{eq} = \frac{k_{un}}{k_{fold}}$$

$$I + I \underset{k_{-1}}{\overset{k_1}{\rightleftarrows}} D$$

$$I + D \underset{k_{-2}}{\overset{k_2}{\rightleftarrows}} T$$

Fig. 7 Scheme of the aggregation process based on a modified Lumnry-Eyring model.

where $[N]$, $[I]$, $[D]$ and $[T]$ are the molar concentrations of native mAb, intermediate species prone to aggregation, dimers and trimers, respectively; k_1 and k_2 are the rate constants for the dimer and trimer formation, respectively; and k_{-1} and k_{-2} are the rate constants for the corresponding backward reactions.

For the experimental techniques applied in this work, it is impossible to distinguish between the N and I species. The experimentally measurable quantity is in fact only the total monomer concentration $[M] = [N] + [I]$, whose mass of the total monomer concentration f, $[I] = f \times [M]$, where $f = K_{eq}/(1 + K_{eq})$. Then, Eqs. 2 to 5 can be re-written using only experimentally measurable quantities as follows:

$$\frac{d[M]}{dt} = -2k_{1,app}[M]^2 + 2k_{-1}[D] - k_{2,app}[M][D] + k_{-2}[T] \tag{6}$$

$$\frac{d[D]}{dt} = k_{1,app}[M]^2 - k_{-1}[D] - k_{2,app}[M][D] + k_{-2}[T] \tag{7}$$

$$\frac{d[T]}{dt} = k_{2,app}[M][D] - k_{-2}[T] \tag{8}$$

where the apparent rate constants, $k_{1,\mathrm{app}} = f^2 \times k_1$ and $k_{2,\mathrm{app}} = f \times k_2$, have been introduced. It is worth noting that such apparent rate constants are composed of two terms describing the two main aspects of the process: the conformational stability behavior of the macromolecule (represented by *f*) and the kinetic colloidal stability of the solution (represented by the intrinsic kinetic constants k_1 and k_2). The two aspects are intrinsically interconnected, and their individual contribution to the aggregation process cannot be distinguished.

The $k_{1,\mathrm{app}}$ value can be evaluated experimentally from the early stage of the aggregation where the only species

present in the system are monomers and dimers, while trimers are negligible. Then, at time $t \rightarrow 0$, Eq. 6 reduces to

$$\left.\frac{d[M]}{dt}\right|_0 = -2k_{1,app} \cdot [M]^2, \tag{9}$$

which can be easily integrated:

$$\frac{1}{[M]} - \frac{1}{[M_0]} = 2k_{1,app} \cdot t, \tag{10}$$

where $[M_0]$ is the given concentration of total monomers at $t=0$. Thus, the plot of $1/[M]$-$1/[M_0]$ *versus* t should be a straight line whose slope gives $k_{1,\mathrm{app}}$. Indeed, this was verified, as shown in Fig. 8, for experimental runs 6, 9 and 10 in Table I.

The other three unknown kinetic parameters, $k_{2,\mathrm{app}}$, k_{-1} and k_{-2}, have been estimated by solving Eqs. 6 to 8 and fitting the experimental data, minimizing an error function. Applying such procedure, it is possible to estimate with uniqueness the kinetic constant k_{-1} and the equilibrium constants $K_{2,eq} = k_{2,app}/k_{-2}$, for the formation of trimers. Details about the fitting procedure can be found in the Supplementary material. The summary of the estimated parameter values is reported in Table II.

It is worth noting that based on the physicochemical meaning of the kinetic rate constants they are not expected to depend on the mAb concentration but to do so for NaCl. Therefore, we fit run 6 in Fig. 9a and then, with the same kinetic parameters, we predict runs 7 and 8 in Fig. 9b (for the sake of simplicity, only time evolutions of the residual monomers are reported). In Fig. 10a the time evolutions of the residual monomers at different salt concentrations fitted by the model using the kinetic parameters in Table II are

Table II Values of the Rate Constants Corresponding to the Kinetic Scheme in Fig. 7 Estimated at Different Salt Concentrations

NaCl Conc [mol/L]	$k_{1,\mathrm{app}}$ [L·mol^{-1}·s^{-1}]	k_{-1} [1·s^{-1}]	$K_{2,eq} = k_{2,app}/k_{-2}$ [L·mol^{-1}]
0.1	5.3	$1.50 \cdot 10^{-4}$	$4.29 \cdot 10^{4}$
0.15	15.5	$1.37 \cdot 10^{-4}$	$1.05 \cdot 10^{5}$
0.3	30	$3.59 \cdot 10^{-5}$	$1.54 \cdot 10^{7}$
0.5	32.5	$3.02 \cdot 10^{-5}$	$5.49 \cdot 10^{7}$

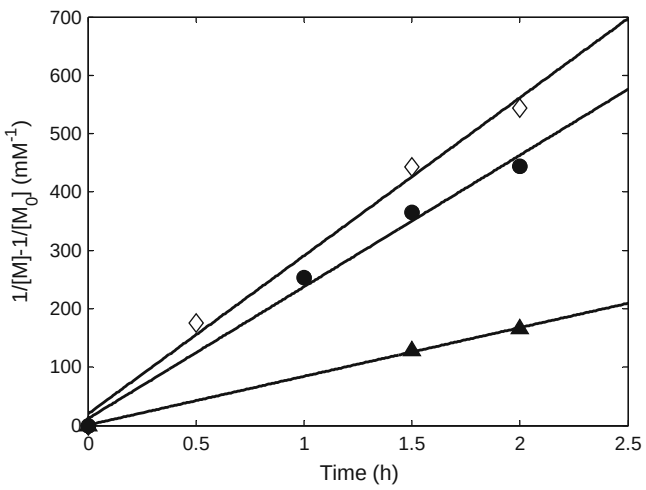

Fig. 8 Monomer conversion, plotted in the form of $1/[M] - 1/[M_0]$ (according to Eq. 10), *versus* time for the 1 g/L mAb solution in 25 mM citric acid buffer at pH 3.0 and different salt concentrations: 0.15 M (▲), 0.3 M (●), 0.5 M (◇) (Runs 6, 9 and 10 in Table I). Continouos lines represent fitting to experimental data.

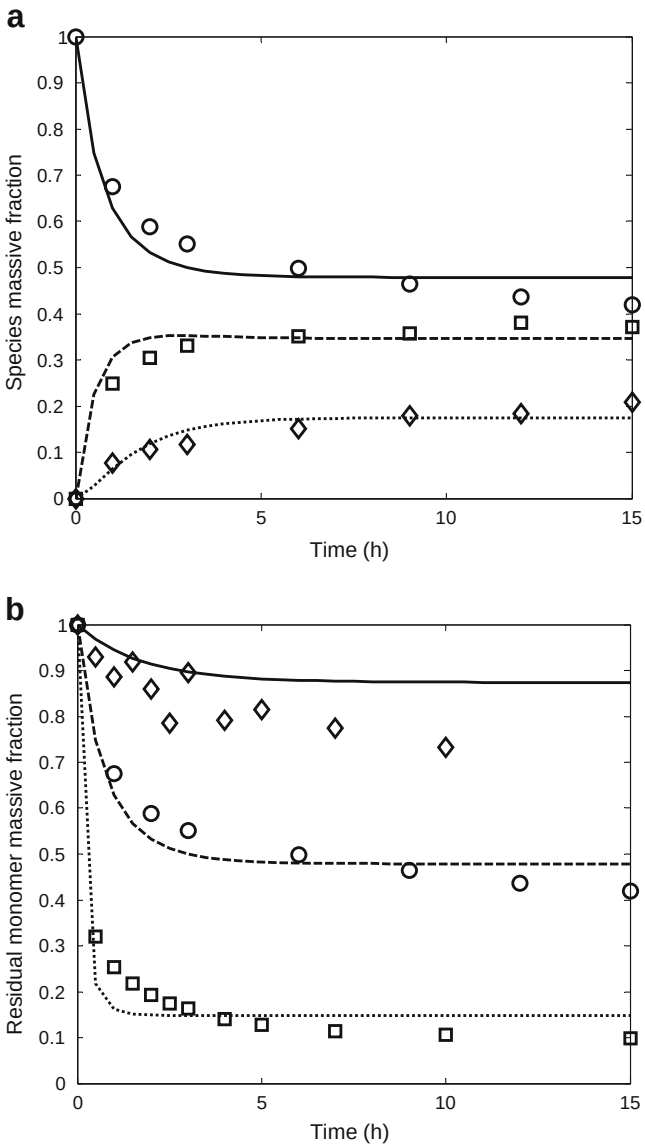

Fig. 9 Comparison between model predictions (continuous curves) and experimental data (symbols). (**a**) Time evolutions of monomer (○), dimer (□) and trimer (◇) mass fractions for run 6 in Table I; (**b**) effect of the mAb concentration on the kinetics: 0.1 g/L (◇), 1 g/L (○), 10 g/L (□) (i.e., Runs 7, 6 and 8 in Table I, respectively).

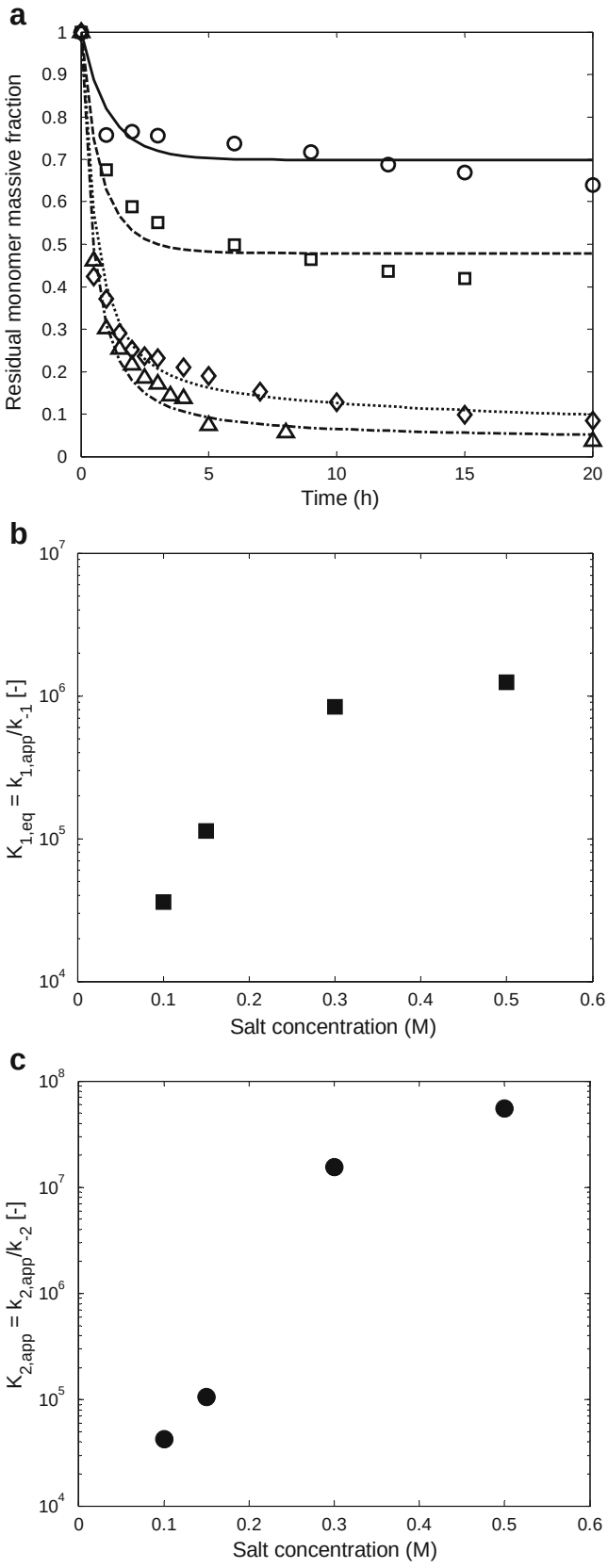

Fig. 10 (**a**) Fitting of the salt effect on the aggregation kinetics by the model (continuous curves), compared with the experimental data (symbols): 0.1 M (○), 0.15 M (□), 0.3 M (◇), 0.5 M (△) (i.e., runs 5, 6, 9 and 10 in Table I, respectively); (**b**) the estimated kinetic parameters for dimer formation in Table II, plotted in the form of $K_{1,eq} = k_{1,app}/k_{-1}$ as a function of the salt concentration, and (**c**) the same as (**b**) but for trimer formation, $K_{2,eq} = k_{2,app}/k_{-2}$.

compared to the experimental results. Again, good agreement has been obtained. It is therefore concluded that the modified Lumry-Eyring model can well represent the aggregation process of the considered mAb systems.

In addition, to better understand the salt effect on the oligomer formation, we plot the equilibrium constants, $K_{1,\mathrm{eq}} = k_{1,\mathrm{app}}/k_{-1}$ and $K_{2,eq} = k_{2,app}/k_{-2}$, for the formation of dimers and trimers, respectively, as a function of salt concentration (Fig. 10b and c). Both $K_{1,\mathrm{eq}}$ and $K_{2,\mathrm{eq}}$ increase monotonically as the salt concentration increases. The data in Table II show that such a trend results from the monotonic increase in the forward reactions and the decrease in the backward reactions as a function of the salt concentration. Although at very low salt concentrations the salt effect may be reasonably explained by protein charge screening by the salt ions as described by the classical DLVO theory (37,38), for the salt concentration investigated in this work (0.1–0.5 M), additional salt effects on system thermodynamics and solvation effects (salting-out) must be considered (4). More specifically, the changes in the system thermodynamics with adding salt are mostly related to anion binding, which reduces electrostatic repulsive forces both intra- and inter-molecularly (39), with two consequences: (1) changes in the secondary structure of the mAb (most likely, the formation of a more reactive intermediate I in the scheme in Fig. 7 is favored), and (2) increase in the possibility for hydrophobic surface patches of two aggregating proteins to come closer. Salting-out effect is related to attractive protein-protein interaction arising from preferential exclusion of the salt from protein-surface and consequent increase of protein-surface free energy (40). Evidently, all these effects go beyond charge screening and DLVO model and are not separable. Nevertheless, on the basis of the analysis above, we can conclude that addition of the salt has two main overall consequences: (1) promoting aggregation (i.e., increasing $k_{1,\mathrm{app}}$ in Table II), and (2) increasing the aggregation-bond strength, thus decreasing the backward reaction rate (k_{-1}). These, in turn, lead to a shift of the equilibria in Fig. 7 towards oligomers formation.

CONCLUSIONS

In the present work, the aggregation (stability) behavior of monoclonal antibody (mAb) solutions has been investigated

under industrial-relevant conditions, typically encountered during purification through protein A chromatography, i.e., acidic conditions and presence of salt (NaCl) in the concentration range of 0.1–0.5 M. The aggregation was followed on-line by dynamic light scattering (DLS), and the oligomer distributions were analyzed off-line through both FFF (field flow fractionations) and SEC (size exclusion chromatography) separation techniques.

It is found that the main parameters affecting mAb aggregation are pH and salt concentration. At pH below 4.0 and in the presence of salt, the antibodies self-associate (aggregate) progressively with time to form small oligomers (e.g., dimers and trimers). The aggregation is accompanied by an increase in the content of the secondary β–sheet structure of the mAb. A lag-phase that is commonly encountered in the aggregation of other similar proteins is not observed here. Even after 1 month, neither macroscopic changes of the solution or precipitation of large aggregates can be observed. The monomers can be recovered from the oligomers by dilution in salt-free solutions, indicating that the aggregates are reversible.

Both the FFF and SEC techniques have been successfully applied to measure the oligomer distributions (i.e., monomer, dimer and trimer), and the results between the two techniques are in good agreement. To support the reliability of the obtained oligomer distributions, we have applied them to reconstruct the time evolution of the average hydrodynamic radius and compared the obtained values to the on-line DLS measurements, and good agreement has been obtained. Thus, the approach applied in this work represents an example of oligomer determination, which may be applied in other protein-aggregation systems to obtain important information about oligomer distribution and reversibility.

The aggregation kinetic data have been interpreted using a modified Lumry-Eyring model, where reversibility has been introduced into the reaction scheme. The key assumption of the model is an initial reversible conformational change resulting in an aggregation-prone intermediate *I*. It is found that with properly estimated parameters, the proposed kinetic model can well predict the time evolution of all the oligomers determined from the FFF and SEC techniques and properly account for the effect of the mAb and salt concentrations on the aggregation kinetics.

ACKNOWLEDGMENTS

Financial support of the Swiss National Science Foundation (Grant No. 200020-126487/1) is gratefully acknowledged. We thank also Merck Serono (Vevey, Switzerland) for supplying the monoclonal antibody and Dr. Silvia Campioni and Prof. Riek (ETH Zurich) for allowing and assisting CD measurements in their labs.

REFERENCES

1. Aggarwal S. What's fueling the biotech engine-2007. Nat Biotechnol. 2008;26:1227–33.
2. Carter PJ. Potent antibody therapeutics by design. Nat Rev Immunol. 2006;6:343–57.
3. Manning MC, Patel K, Borchardt RT. Stability of protein pharmaceuticals. Pharm Res. 1989;6:903–18.
4. Chi EY, Krishnan S, Randolph TW, Carpenter JF. Physical stability of proteins in aqueous solution: mechanism and driving forces in nonnative protein aggregation. Pharm Res. 2003;20:1325–36.
5. Wang W. Protein aggregation and its inhibition in biopharmaceutics. Int J Pharm. 2005;289:1–30.
6. Cromwell MEM, Hilario E, Jacobson F. Protein aggregation and bioprocessing. Aaps Journal. 2006;8:E572–9.
7. Mahler H-C, Friess W, Grauschopf U, Kiese S. Protein aggregation: pathways, induction factors and analysis. J Pharm Sci. 2009;98:2909–34.
8. Braun A, Kwee L, Labow MA, Alsenz J. Protein aggregates seem to play a key role among the parameters influencing the antigenicity of interferon alpha (IFN-alpha) in normal and transgenic mice. Pharm Res. 1997;14:1472–8.
9. Rosenberg AS. Effects of protein aggregates: an immunologic perspective. AAPS J. 2006;8:E501–7.
10. Hartmann WK, Saptharishi N, Yang XY, Mitra G, Soman G. Characterization and analysis of thermal denaturation of antibodies by size exclusion high-performance liquid chromatography with quadruple detection. Anal Biochem. 2004;325:227–39.
11. Fesinmeyer RM, Hogan S, Saluja A, Brych SR, Kras E, Narhi LO, *et al.* Effect of ions on agitation- and temperature-induced aggregation reactions of antibodies. Pharm Res. 2009;26:903–13.
12. Kiese S, Papppenberger A, Friess W, Mahler HC. Shaken, not stirred: mechanical stress testing of an IgG1 antibody. J Pharm Sci. 2008;97:4347–66.
13. Bee JS, Stevenson JL, Mehta B, Svitel J, Pollastrini J, Platz R, *et al.* Response of a concentrated monoclonal antibody formulation to high shear. Biotechnol Bioeng. 2009;103:936–43.
14. Kueltzo LA, Wang W, Randolph TW, Carpenter JF. Effects of solution conditions, processing parameters, and container materials on aggregation of a monoclonal antibody during freeze-thawing. J Pharm Sci. 2008;97:1801–12.
15. Curtisand RA, Lue L. A molecular approach to bioseparations: protein-protein and protein-salt interactions. Chem Eng Sci. 2006;61:907–23.
16. Stefaniand M, Dobson CM. Protein aggregation and aggregate toxicity: new insights into protein folding, misfolding diseases and biological evolution. J Mol Med-Jmm. 2003;81:678–99.
17. Wasmer C, Lange A, Van Melckebeke H, Siemer AB, Riek R, Meier BH. Amyloid fibrils of the HET-s(218–289) prion form a beta solenoid with a triangular hydrophobic core. Science. 2008;319:1523–6.
18. Chennamsetty N, Helk B, Voynov V, Kayser V, Trout BL. Aggregation-prone motifs in human immunoglobulin G. J Mol Biol. 2009;391:404–13.
19. Shukla AA, Gupta P, Han X. Protein aggregation kinetics during Protein A chromatography Case study for an Fc fusion protein. J Chromatogr A. 2007;1171:22–8.
20. Chennamsetty N, Voynov V, Kayser V, Helk B, Trout BL. Design of therapeutic proteins with enhanced stability. Proc Natl Acad Sci USA. 2009;106:11937–42.
21. Shuklaand AA, Hinckley P. Host cell protein clearance during protein a chromatography: development of an improved column wash step. Biotechnol Prog. 2008;24:1115–21.
22. Carpenter JF, Randolph TW, Jiskoot W, Crommelin DJA, Middaugh CR, Winter G. Potential inaccurate quantitation

and sizing of protein aggregates by size exclusion chromatography: essential need to use orthogonal methods to assure the quality of therapeutic protein products. J Pharm Sci. 2010;99:2200–8.
23. Lumryand R, Eyring H. Conformation changes of proteins. J Phys Chem. 1954;58:110–20.
24. Roberts CJ. Kinetics of irreversible protein aggregation: analysis of extended Lumry-Eyring models and implications for predicting protein shelf life. J Phys Chem B. 2003;107:1194–207.
25. Morris AM, Watzky MA, Finke RG. Protein aggregation kinetics, mechanism, and curve-fitting: a review of the literature. Biochim Et Biophys Acta Proteins Proteomics. 2009;1794:375–97.
26. Khurana R, Gillespie JR, Talapatra A, Minert LJ, Ionescu-Zanetti C, Millett I, *et al.* Partially folded intermediates as critical precursors of light chain amyloid fibrils and amorphous aggregates. Biochemistry. 2001;40:3525–35.
27. Uversky VN. Mysterious oligomerization of the amyloidogenic proteins. FEBS J. 2010;277:2940–53.
28. Bellotti V, Mangione P, Merlini G. Review: immunoglobulin light chain amyloidosis - The archetype of structural and pathogenic variability. J Struct Biol. 2000;130:280–9.
29. Leeman M, Wahlund KG, Wittgren B. Programmed cross flow asymmetrical flow field-flow fractionation for the size separation of pullulans and hydroxypropyl cellulose. J Chromatogr A. 2006;1134:236–45.
30. Vermeerand AWP, Norde W. The thermal stability of immunoglobulin: unfolding and aggregation of a multi-domain protein. Biophys J. 2000;78:394–404.
31. Lattuada M, Wu H, Morbidelli M. Hydrodynamic radius of fractal clusters. J Colloid Interface Sci. 2003;268:96–105.
32. Grillo AO, Edwards KLT, Kashi RS, Shipley KM, Hu L, Besman MJ, *et al.* Conformational origin of the aggregation of recombinant human factor VIII. Biochemistry. 2001;40:586–95.
33. Kendrick BS, Carpenter JF, Cleland JL, Randolph TW. A transient expansion of the native state precedes aggregation of recombinant human interferon-gamma. Proc Natl Acad Sci USA. 1998;95:14142–6.
34. Finke JM, Roy M, Zimm BH, Jennings PA. Aggregation events occur prior to stable Intermediate formation during refolding of interleukin 1 beta. Biochemistry. 2000;39:575–83.
35. Foguel D, Robinson CR, de Sousa PC, Silva JL, Robinson AS. Hydrostatic pressure rescues native protein from aggregates. Biotechnol Bioeng. 1999;63:552–8.
36. Moore JMR, Patapoff TW, Cromwell MEM. Kinetics and thermodynamics of dimer formation and dissociation for a recombinant humanized monoclonal antibody to vascular endothelial growth factor. Biochemistry. 1999;38:13960–7.
37. Zhangand YJ, Cremer PS. Interactions between macromolecules and ions: the Hofmeister series. Curr Opin Chem Biol. 2006;10:658–63.
38. Broeringand JM, Bommarius AS. Evaluation of Hofmeister effects on the kinetic stability of proteins. J Phys Chem B. 2005;109:20612–9.
39. Goto Y, Calciano LJ, Fink AL. Acid-induced folding of proteins. Proc Natl Acad Sci USA. 1990;87:573–7.
40. Curtis RA, Prausnitz JM, Blanch HW. Protein-protein and protein-salt interactions in aqueous protein solutions containing concentrated electrolytes. Biotechnol Bioeng. 1998;57:11–21.